

Post-impact residual torsional strength and acoustic emission analysis of filament wound composite pipes

Karolina Paczkowska¹⁾, *) (0009-0007-4170-3406), Zuzanna Pacholec¹⁾ (0009-0002-4384-0344), Grzegorz Szychta¹⁾, Wojciech Błażejewski¹⁾ (0000-0001-9260-1388), Paweł Stabla¹⁾ (0000-0001-6891-582X), Michał Barcikowski¹⁾ (0000-0001-5135-7892)

DOI: <https://doi.org/10.14314/polimery.2025.1.4>

Abstract: The residual torsional strength of composite pipes after different impact loading and torsional strength with acoustic emission analysis were investigated. It was shown that the residual torsional strength of composite pipes and the strength of undamaged samples differ significantly depending on the fiber winding angle. The undamaged pipes with a winding angle of 45° showed higher torsional strength compared with the samples with an angle of 30°.

Keywords: filament winding, residual torsional strength, acoustic emission, composite pipes, non-destructive tests.

Poudarowa wytrzymałość resztkowa na skręcanie i analiza emisji akustycznej nawijanych rur kompozytowych

Streszczenie: Zbadano wytrzymałość resztkową na skręcanie rur kompozytowych po różnym obciążeniu udarowym oraz wytrzymałość na skręcanie z analizą emisji akustycznej. Wykazano, że wytrzymałość resztkowa rur kompozytowych na skręcanie oraz wytrzymałość próbek nieuszkodzonych różni się znacznie w zależności od kąta nawijania włókien. Nieuszkodzone rury o kącie nawijania 45° wykazały większą wytrzymałość na skręcanie w porównaniu z próbami o kącie nawijania 30°.

Słowa kluczowe: technologia nawijania, wytrzymałość szczątkowa na skręcanie, emisja akustyczna, rury kompozytowe, badania nieniszczące.

Composite materials, while widely valued for their high strength-to-weight ratio and adaptability, have a notable drawback: their considerable susceptibility to compressive and impact loading [1–3]. Impact loading, in particular, poses a significant risk, as even low-energy impacts can cause severe damage within the material [4]. Assessing this damage is often challenging, as defects may form and propagate beneath the surface, making it difficult to detect without specialized instruments [5]. Moreover, when composite components bear substantial loads, their strength can drop rapidly once critical thresholds are surpassed, leading to abrupt and catastrophic failure. Consequently, even minor incidents require careful inspection to ensure the component's integrity [6–8].

Residual strength, as defined within fracture mechanics, describes the material's capacity to withstand further loading despite existing defects. Composite shafts and pipes are particularly affected by that issue. Compared to steel shafts, the advantage of composite

shafts is their lower mass, which reduces the moment of inertia and allows for the use of lighter, less costly bearings. However, even minor damage in these composite elements, especially under high torsional loads, can lead to accelerated failure [9]. Therefore, in the study, the residual torsional strength of composite pipes subjected to impact and torsional loading were investigated.

Impact loading results in three distinct damage mechanisms, determined by the velocity of the impacting element. At velocities well below the ballistic threshold, the impactor rebounds from the surface, transferring only a portion of its energy to the target. At intermediate velocities, the impactor penetrates the target, delivering its full energy. At velocities exceeding the ballistic threshold, the impactor has sufficient energy to perforate the specimen, resulting in full penetration of the target. In this case, a portion of the impactor's energy is dissipated through friction between the impactor and the specimen [10].

There are numerous publications concerning studies on the torsional strength of composite pipes, providing detailed analyses of the stress and strain behaviors [11–14]. Soykök examined the effect of deliberately introduced defects on the structural integrity, compared two

¹⁾ Department of Mechanics, Materials and Biomedical Engineering, Wrocław University of Science and Technology, ul. Smoluchowskiego 25, 50–370 Wrocław, Poland.

*) Author for correspondence: karolina.paczkowska@pwr.edu.pl

different stacking sequences of filament wound glass/epoxy pipes and conducted a parametric examination of fiber winding angles and slot lengths [11]. Chang *et al.* investigated that the composite pipe exhibits nonlinear progressive damage under tensile loads, brittle failure under pure torsional loads, and a combination of both under tension-torsion loading [12]. Mansour *et al.* and Soykök *et al.* conducted both experimental and numerical analyses of the torsional behavior of composite pipes manufactured in filament winding technology [13, 14]. However, there is limited knowledge regarding residual torsional strength. Minak *et al.* investigated residual torsional strength of laminated carbon/epoxy composite pipes after low-velocity impact [15]. Study showed that the residual torsional strength is influenced by the local buckling load of the single laminae or by the maximum strength of the sublaminates. The authors analyzed the impact of the preload on the residual torsional strength, indicating that residual torsional strength decreases as the preload increases. Soykök *et al.* also studied the residual torsional strength of composite pipes [16]. Their study showed that a winding angle of 45° performed best for non-impacted pipes, while 30° and 60° angles exhibited significantly lower maximum torsional moments. After a 2.5 J impact, the 45° and 30° winding angles performed equally, whereas a 7.5 J impact made the 30° pipes perform best. Despite the foundational insights provided by Minak *et al.* [15] and Soykök *et al.* [16], their findings on residual torsional strength have not been widely revisited or expanded upon, leaving a significant gap in the exploration of this topic. Research on residual torsional strength of composite pipes has not been extensively pursued. Quasi-static tests of specimens subjected to impact are more common. Depending on the typical operating conditions expected for the tested material, samples may be subjected to tensile tests [17–19], compression tests [20–22] flexural tests [23–25] or indentation tests [18]. Flexural tests are easier to conduct than compressive, don't need special equipment and are not laden with uncertainties associated with compressive tests [26]. Günöz *et al.* conducted research on the low-velocity impact strength of composite plates [27]. Targino *et al.* investigated the damage tolerance after impact of composite laminates [28]. Barcikowski and Królikowski investigated impact damage and residual flexural strength in glass/polyester laminates [29]. The authors of research [30] studied the impact and flexural behaviors of composite sandwich panels. They used the three-point flexure method to apply loads to the specimens. This study showed that the failure mode of the sandwich specimens was a brittle extrusion on the side of face sheets with a small displacement. However, research on residual torsional strength of composite pipes has not been extensively pursued.

In the evaluation of damage in composites, non-destructive testing (NDT) methods are particularly valuable for detecting and analyzing internal flaws without compromising material integrity. Acoustic emission (AE)

testing is particularly useful in composites, as they consist of multiple components, each emitting characteristic frequency ranges during damage [31]. The identified frequency ranges differ slightly across various publications. Signals associated with matrix damage fall within the range of 90–180 kHz, while fiber damage emits signals at frequencies above 300 kHz. This method also allows for the identification of the specific type of damage occurring at a given moment. Fiber breakage generates signals at frequencies of approximately 400–500 kHz. The frequency range of 180–240 kHz corresponds to fiber-matrix debonding, while the range of 240–300 kHz suggests damage in the form of fiber pull-out from the matrix and delamination [32–34]. Torsional tests of composite pipes were conducted by Hemanth Raj *et al.* [35] where the damage mechanisms of different matrixes were compared using acoustic emission. AE utilizes piezoelectric sensors, which convert acoustic waves into an electrical signal, which is transmitted to the measurement system. Accurate localization of signal sources requires usage of at least two sensors.

The aim of the study is to examine the effect of the winding angle of glass/epoxy thin-walled composite pipes on their residual torsional strength. Additionally, acoustic emission testing was conducted to detect and analyze defects that are not externally visible during torsional strength testing or induction by impact loading. This non-destructive testing method provides insights into internal damage mechanisms and the progression of defects under various loading conditions. This dual approach, residual strength testing and acoustic emission monitoring, aims to enhance both the detection and assessment of damage in composite pipes, providing insights that could inform the design, maintenance, and safety of composite structures in high-stress applications.

EXPERIMENTAL PART

Materials

The composite pipes were manufactured using Vetrotex P185-EC14 E (tex 2400) glass fiber (R&G Faserverbundwerkstoffe GmbH, Waldenbuch, Germany) and Araldite LY 1564 SP epoxy resin with Aradur 3486 hardener (Huntsman, Basel, Switzerland). The resin has a viscosity of 1200–1400 mPa s (at 25°C), which makes it suitable for winding processes. In combination with the hardener, it creates a mixture with a viscosity of 200–300 mPa s (at 25°C) and a gel time of 110–130 minutes (at 60°C). For a 100 g mixture, polymerization occurs within 560–620 minutes. At a later stage, Epidian 6 resin with Z-1 hardener (Sarzyna Chemicals, Nowa Sarzyna, Poland) was used to connect the wooden pins with the wound pipes in a mass ratio of 50:6.5. The use of a different resin was due to the need to obtain higher viscosity and shorter polymerization time (gel time 33 min for Epidian 6).

Composites fabrication

Filament winding

Filament winding (FW) is commonly used to produce rotationally symmetric components with closed surfaces because these geometries maximize the advantages of this technique. The resulting components are typically hollow, which facilitates the removal of the core during production. The core serves as a mandrel on which the resin-impregnated fibers are wound, and its geometry defines the final shape of the composite product.

The samples were prepared using a 4-axis filament winder MAW 20 LS4/1 (Mikrosam, Prilep, Macedonia) (Fig. 1) in a wet-winding process. The tubular samples were produced on a steel mandrel with a diameter of 40 mm and a length of 1000 mm. The resin-impregnated fibers were wound at an angle of 30° for one set of samples and 45° for the other with two layers of wrapping. The angles were selected based on theoretical calculations of stress distribution. The angle of 45° is the theoretically most effective angle for torsional stress on a cylindrical pipe [36, 37], which was confirmed in the study by Fang et al. [38]. The angle of 30° was selected for comparison after Duda *et al.* [37], Morozov [36] and Soykök *et al.* [16]. The average wall thickness of the pipes is 1.3 mm regardless of the winding angle.

After completing the composite winding, the pipes were cured, and once the resin was cross-linked, they were removed from the mandrels and cut into 200 mm specimens.

Reinforcement of the gripping section

The gripping sections of the specimens were reinforced with wooden inserts of 50 mm length to protect against damage. The wooden inserts were further strengthened with E-glass fibers impregnated with resin and bonded into the specimens using Epidian 6 resin. The external surface of the gripping sections was additionally reinforced



Fig. 1. Manufacturing of specimens

with continuous E-glass fibers impregnated with resin. The reinforced specimens were then cured to achieve resin cross-linking. Fig. 2 presents the sample with dimensions.

Methods

The sample sets for each winding angle (30° and 45°) were subjected to impact loading using two devices: a drop-weight impact tester and a pendulum impact tester. Both methods involve lifting a mass to a certain height, releasing a lock, and allowing the impactor to fall freely under the influence of gravity to strike the sample. Additionally, a set of samples for each winding angle was evaluated for damage using a pneumatic cannon to compare impacts characterized by wave propagation typical of small masses and high velocities. Following the impact tests, torsional strength testing was performed on both the damaged samples and undamaged reference samples. The torsion tests were conducted following ASTM D5448/D5448M-11 with adjustments tailored to the experimental framework to evaluate the torsional behaviors of impacted and non-impacted composite pipes manufactured by filament winding. AE testing was additionally conducted on the undamaged samples.

Drop-weight impact

For impact testing used drop-weight impact tester DW1000 (STEP Lab, Treviso, Italy). The first step involved selecting the impact energy for the specimen to achieve visible delamination without penetration or cracking through the entire wall thickness. The tests were conducted on a separate set of specimens. Specimens were supported on two prisms, each 50 mm wide, with a plastic mass as a buffer to dampen at the supports, leaving 100 mm test length in the middle. The impactor tip was hemispherical with 9.0 mm diameter. At an impact energy



Fig. 2. Composite pipe sample



Fig. 3. Modified Charpy impact hammer

of 35 J, penetration occurred, while energies above 20 J resulted in cracking. For energies below 20 J, only minor delamination was observed. Based on these results, an impact energy of 20 J was chosen for the test campaign.

Charpy impact

The second set of samples was subjected to impact loading using a modified Charpy pendulum hammer to obtain an impact energy of 26 J. (Fig. 3) and impacting

point analogue to other methods. Specimens were supported in a prism as in 2.3.1. The pendulum tip was hemispherical and had a diameter of 9.0 mm.

Pneumatic cannon impact test

In the impact test using a pneumatic cannon, a steel bullet with a diameter of 9.0 mm and a weight of 3.0 g was used as the impactor. The projectile velocity was measured using a Shooting Chrony M1. Based on these measurements, the impact energy (35 J) was calculated. The measuring system and schematic of the pneumatic cannon for impact testing are presented in Fig. 4. Specimens were supported in two prisms, leaving 100 mm test length in the middle.

Torsional strength

The schematic of the measurement system for torsional strength testing is presented in Fig. 5. The torsional moment and the twist angle were measured during the strength tests. One end of the specimen was clamped immobile. The other end related to a freely rotating arm, at the end of which a progressively increasing load (F) was applied.

Acoustic emission

AE tests were conducted on two specimens, with winding angles of 30° and 45° during torsional strength testing using the measurement system (Fig. 5). During the AE tests, the specimens were loaded with progressively growing torque from 0 to 150 Nm, the aim was to maintain the specimens structurally intact without causing complete failure. Each specimen was equipped with four AE sensors, arranged in two pairs aligned on opposite sides (Fig. 6). The four sensors were used to attempt to locate the occurrence of signal-emitting events. This process allows for the precise determination of the location of the emission signal. The Vallen AMSY-6 AE monitoring system (Vallen Systeme GmbH, Wolfratshausen, Germany) consists of a multi-channel data acquisition module, transducers, preamplifiers, and software that enables the recording of selected parameters.

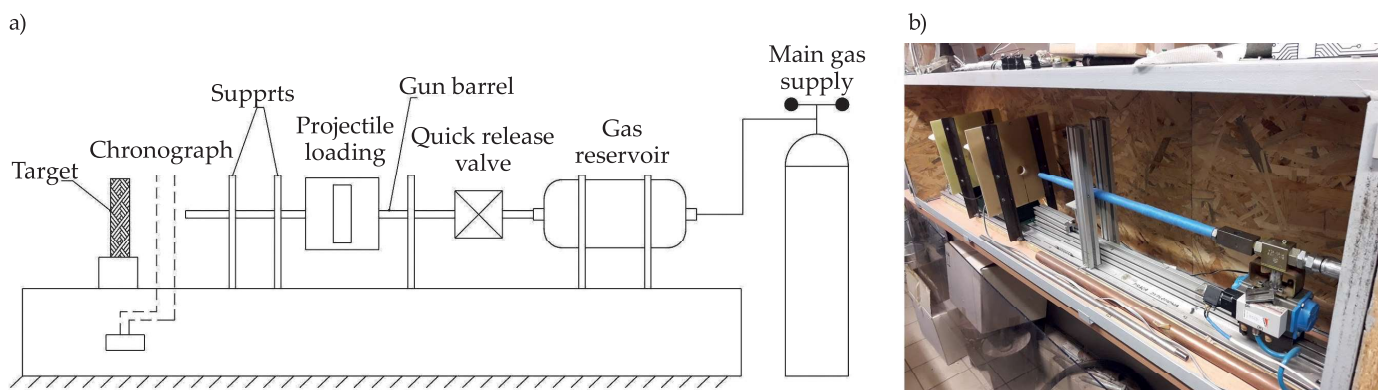


Fig. 4. Pneumatic cannon: a) a schematic diagram, b) view of the test stand

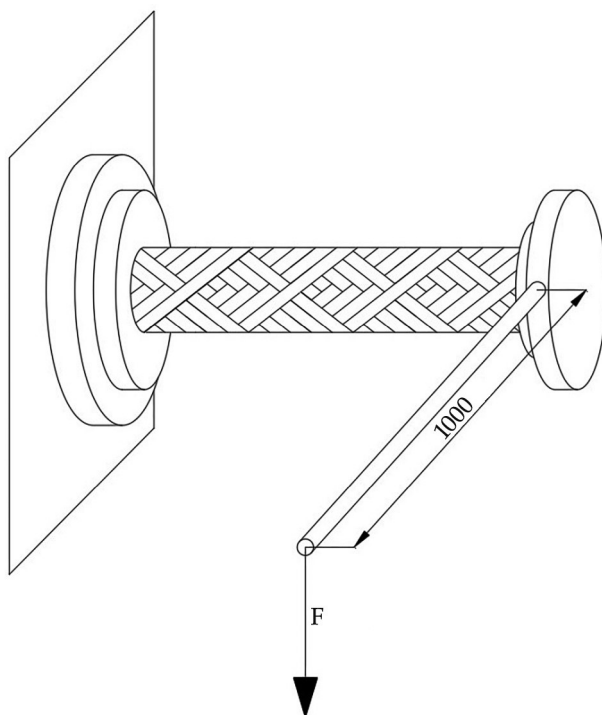


Fig. 5. Schematic of the test setup for torsional strength testing

RESULTS AND DISCUSSION

Impact and torsional strength analysis

The extent of delamination was used as a measure of the damage to the specimens for each angle and for each type of impact load. The delamination area was determined using transmitted light optical analysis. The actual delamination area was calculated using ImageJ software. Table 1 shows examples of delamination areas for specimens from each test set, along with the average calculated delamination area and average torque for each specimen set.

Delamination, concentrated around the fibers, and perforation are more pronounced in specimens subjected to low-velocity high-mass impacts. In this group, defects are more visible due to increased light absorption, which is also associated with a higher number of microcracks in the affected area. In contrast, for specimens impacted using the pneumatic cannon, the damage covers a significantly larger area, and the delamination is more dispersed due to the penetrating wave generated by the higher impact velocities.

Despite the smaller delamination areas observed in specimens with a 30° winding angle (8% for drop-weight, 35% for Charpy, 9% for pneumatic cannon) than in specimens with a 45° winding angle, it can be concluded that 30° angle exhibits lower tolerance to impact damage, since the impactor penetrated through the walls of all specimens. On the other hand, specimens with a 45° winding angle were able to absorb the energy of multiple subsequent impacts, as the impactor rebounded several times, dissipating the residual energy from the impact



Fig. 6. AE testing of torqued composite pipe

impulses. For specimens with a 30° winding angle, the delamination areas were comparable between the tests conducted using the Charpy and the drop-weight impact testers, differing by 7%. However, in the case of specimens with a 45° winding angle, the delamination area significantly increased (by 31%) when subjected to the Charpy impact test due to slightly higher impact energy compared to the drop-weight impact test.

Higher residual torsional strength was observed in pipes with a 30° winding angle than 45° winding angle (70% for drop-weight, 1% for Charpy, 18% for pneumatic cannon), despite the weakening of the walls caused by perforation. However, undamaged specimens exhibited higher torsional strength at a 45° winding angle rather than 30° by 56%. For pipes with a 30° winding angle, the fibers are aligned at a shallower angle relative to the applied impact force, which can result in more efficient energy absorption during the impact. The lower winding angles may result in a more diffuse stress distribution around delaminated regions, allowing the remaining intact fibers to better bear the applied torsional load. In the 45° winding angle pipes, the fibers are more aligned with the direction of shear stress during torsion. At the same time, fiber wounds according to stress distribution may make them more sensitive to discontinuities caused by impact damage. On the other hand, compliance of winding angle with stress distribution (45°) in undamaged samples results in efficient transmission of shear forces by fibers and thus higher torsional strength.

During torsional tests, all specimens damaged due to micro-buckling (kinking), which is characterized by the bending of fiber bundles under compressive forces (Fig. 7). Kinking forms when a group of fibers lose structural integrity with the polymer matrix, weakened due to yielding and cracking under shear stresses. Once a kink-band develops, the fibers undergo simultaneous rotation [39]. During kink-band initiation and propagation, fibers aligned with the loading direction experience significant compressive stress and undergo unstable rotation induced by inter-fiber shear stress [40]. Study [41] indicate, that kinking is affected also by the shear properties of the matrix, since the matrix accommodate the deformation of the fibers. L. Xun *et al.* studied torsional damage mechanisms in 3D composite pipes braided with carbon fibers reinforced with epoxy resin. They developed multiscale equivalent models by com-

Table 1. Impact strength and residual torsional strength of composite pipes

Type of impact load	Impact energy, J	Winding angle	Delamination area	Delamination outline	Delamination area, cm ²	Torque, Nm
Reference (no load)	—	30° 45°	— —	— —	— —	402.84 630.04
Drop-weight impact	20	30°			8.67	144.20
		45°			9.44	84.81
Charpy impact	26	30°			8.10	85.87
		45°			12.39	84.73
Pneumatic cannon	35	30°			42.48	141.61
		45°			46.55	119.73

bining mesoscopic and homogenous structures. Studies showed that cracking had been the main damage mode. Failure in the form of buckling of specimens led to stress concentration in interlacing points of braided fibers [42]. Chang *et al.* investigated the torsional loading behavior of carbon/epoxy composite pipes. Their study identified

three distinct stages during the loading process. The first stage is linear, reaching a maximum load point (approximately 100 Nm) before a sudden failure, while the second stage exhibits stabilized curves. The third stage leads to the final failure of the specimens. The authors observed no significant changes on the surface of specimens, but

a)



b)

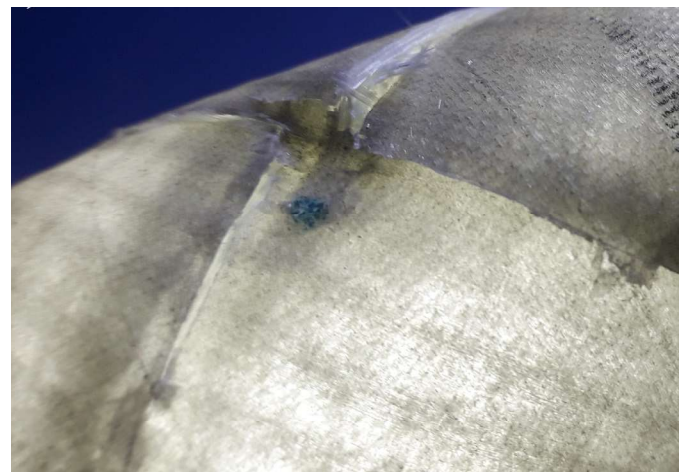


Fig. 7. Residual torsional strength test samples with the damage resulted from the kinking mechanism: a) sample with a through-hole and delamination after impact, b) specimen with delamination only

cracks along the mosaic pattern directions appeared as the load approached the peak value. Their findings suggest that the failure process of torsional loading involves the collapse of the matrix within fiber bundles, leaving monofilaments to bear the load, while undulated fiber bundles in the winding direction are compressed, and those in the opposite direction are transversely stretched, leading to matrix cracking and shear failure during torsion [12]. Mansour *et al.* conducted torsional loading tests for glass/epoxy and carbon/epoxy composite tubular specimens. Maximum torque values of 191 Nm for carbon fiber pipes and 220 Nm for glass fiber pipes [13]. Soykök *et al.* examined the behavior of thin-walled hollow cylindrical glass/epoxy composite pipes and found that specimens with a 45° winding angle exhibited the highest average torsional resistance (27 Nm) [14]. The mean torque results of this study are consistent with findings from other studies regarding torsional loading. However, direct comparison of numerical values is challenging due to diverse types of materials, layers configurations, mosaic patterns and winding angles employed by different authors. In contrast to these works, the present research focused on the influence of winding angles on residual torsional strength and failure mechanisms following impact loading.

Acoustic emission

The conducted research results are presented in the form of graphs comparing various variables for both specimens. Based on these graphs, it is possible to identify the processes that occurred during the loading of the specimens. There was an attempt to locate the AE events on specific points of the surface. In the case of the filament-wound composite, the signal travels most easily along the fibers, causing significant differences in the velocities detected by the sensors. As a result, the software struggled to accurately locate the origin of the signal for

the tested composite pipes; it was not possible to achieve accurate localization due to their wound structure and the presence of interwoven fibers.

Fig. 8 shows the RMS along with a curve illustrating the cumulative number of AE events. The graph is divided into three periods: A, B, and C. During period A, there were few events with low RMS values. At around 60 seconds, at the beginning of period B, there was a significant increase in acoustic emission events with greater intensity and higher frequency. This phase marks the initiation and progression of microcracks in the composite, caused by the applied torsional moment. In period C, the RMS values decreased, and the number of AE events also ceased to grow drastically. The beginning of phase C corresponds to the point where the maximum torsional load was reached. After that, the load was no longer increased, and the specimen was left to stabilize. The stabilization process is evident as a reduction in the strength and frequency of signals shown on the graph.

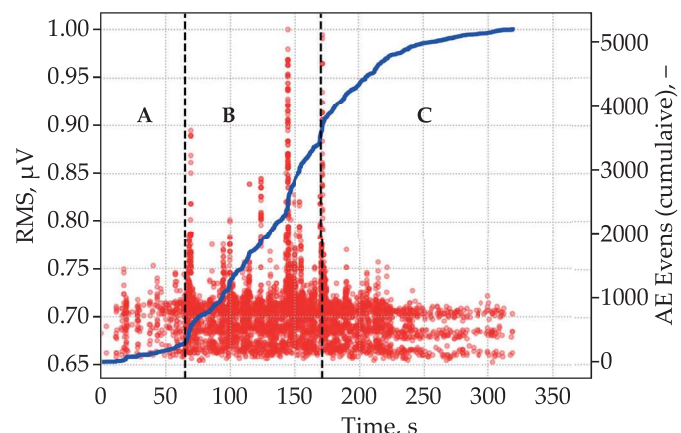


Fig. 8. RMS and cumulative AE events as a function of time for 30° winding angle

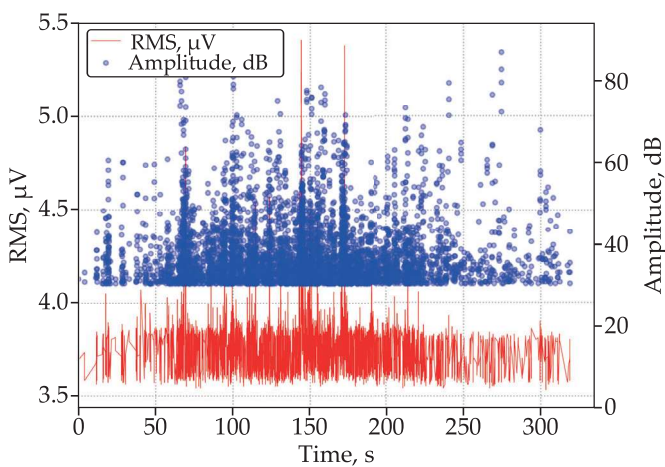


Fig. 9. RMS and amplitude as a function of time for 30° winding angle

In Fig. 9 it can be observed that in the initial phase, the signal amplitude fluctuates between 20 and 50 dB. Subsequently, in correlation with the increase in RMS, the amplitude also rises to approximately 80 dB. According to [43], amplitudes in the range of 48-58 dB are characteristic of resin cracking, suggesting that this phenomenon occurs in the first loading phase. Amplitude values in the range of 50-80 dB is associated with fiber-matrix debonding in the composite. Signals with amplitudes between 80-100 dB indicate fiber breakage. Fig. 9 shows that such events are the least numerous, indicating that significant structural damage to the composite did not occur during loading. Once the load was stabilized at 150 Nm, the RMS signal quickly decreased to about 3.8 μ V, and the amplitude of the signals also dropped. However, some high-amplitude events still appeared, suggesting the propagation of structural damage.

For the 45° specimen an analogous graph was obtained (Fig. 10). The loading process for this sample was longer than for the 30° one which caused more AE events to be registered. Similar observations can be made to the previous sample about the registered amplitudes. However,

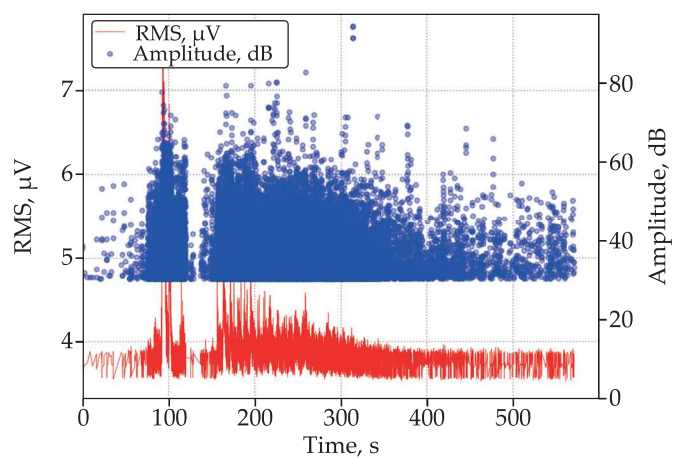


Fig. 10. RMS and amplitude as a function of time for 45° winding angle

there are less AE events over 80 dB, indicating that fiber breakage was less frequent.

In the frequency versus amplitude plot of the AE signals for the sample with a winding angle of 30° (Fig. 11), it can be observed, similarly to the amplitude-time plot (Fig. 9), that most of the events had an amplitude below 60 dB in all frequency bands. The most numerous events were those with a frequency of 150-200 kHz and an amplitude of 30-40 dB, which are signals indicative of resin cracking. A few events occurred with a frequency above 400 kHz, suggesting reinforcement fiber damage; however, these events were rare, indicating that the failure of the specimen was primarily matrix driven.

In the plot for the sample with a winding angle of 45° (Fig. 12), it can be observed that the obtained frequencies reached approximately 550 kHz suggesting fiber breakage. Similarly to the previous sample, most EA events occurred at a frequency of around 150 kHz, indicating matrix cracking. Therefore, the failure mode may be identified as predominantly matrix driven.

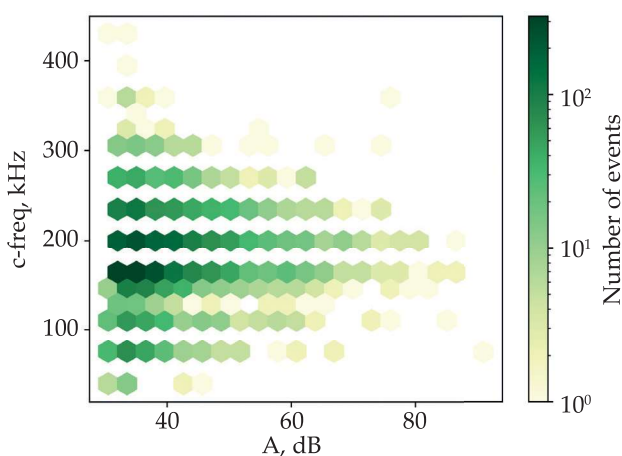


Fig. 11. Frequency as a function of amplitude for 30° winding angle

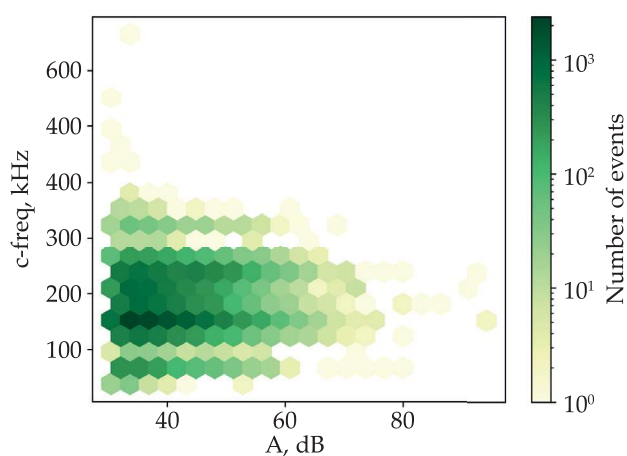


Fig. 12. Frequency as a function of amplitude for 45° winding angle

CONCLUSIONS

This paper presents the results of an experimental study to investigate the effect of winding angles on the residual torsional strength and damage mechanisms of glass-epoxy composite pipes using AE as a non-destructive evaluation method. The specimen was designed to minimize stress concentration in the gripping region and ensure that the final failure occurs in the working section. The pipes were manufactured using a filament winding process. Three types of impact loading were applied to access the material response. The delamination area and residual torsional strength were evaluated, providing insight into the effect of impact damage. AE analysis of the twisted pipes was also presented to further investigate the damage mechanism.

The samples with a 30° winding angle exhibited higher residual torsional strength compared to those with a 45° winding angle. This could be attributed to the more effective dispersion of stress around the delaminated regions post-impact.

At the same time, the samples with a winding angle of 30° have lower resistance to damage caused by axial impact. The undamaged pipes with a winding angle of 45° showed higher torsional strength compared with the samples with an angle of 30°, indicating that the fibers were more aligned with the stress distribution under torsional loading.

The failure mechanism in all torsional tests was kinning, characterized by fiber bending and debonding from the matrix. This corresponds to the results obtained from the AE tests where specific signals corresponding to matrix cracking and fiber matrix debonding along with limited fiber breakage were detected in both samples.

Authors contribution

K.P. – research concept, investigation, visualization, writing-original draft, writing-review and editing; Z.P. – investigation, validation, writing-original draft, writing-review and editing; G.S. – investigation, validation; W.B. – methodology, investigation, validation, supervision; P.S. – methodology, supervision; M.B. – research concept, visualization, writing-review and editing.

Funding

No funding/no source of financing.

Conflict of interest

The authors declare that they have no known competing financial interests or personal relationships that could have appeared to influence the work reported in this paper.

Data availability

Data will be made available on request.

Copyright © 2025 The publisher. Published by Łukasiewicz Research Network – Industrial Chemistry Institute. This article is an open access article distributed under the terms and conditions of the Creative Commons Attribution (CC BY-NC-ND) license (<https://creativecommons.org/licenses/by-nc-nd/4.0/>).



REFERENCES

- [1] Md Shah A.U., Hameed Sultan M.T., Safri S.N.A.: *Polymers* **2020**, 12(6), 1288.
<https://doi.org/10.3390/polym12061288>
- [2] Ahmad M., Feng D., Ali W.: *European Journal of Applied Science, Engineering and Technology* **2024**, 2(3), 59.
[https://doi.org/10.59324/ejaset.2024.2\(3\).06](https://doi.org/10.59324/ejaset.2024.2(3).06)
- [3] Pham D. C., Lua J., Zhang D.: "3D Progressive Failure Modeling of Drop-Weight Impact on Composite Laminates", Materials from ASC 33rd Annual Technical Conference, 2018.
<https://doi.org/10.12783/asc33/25904>
- [4] Razali N., Sultan M.T.H., Mustapha Bin F. et al.: *The International Journal of Engineering and Science* **2014**, 3(7), 2319.
- [5] Seamone A., Davidson P., Waas A.M.: *AIAA SCITECH 2023*, 2023, 1904.
<https://doi.org/10.2514/6.2023-1904>
- [6] Liu H., Liu J., Zhou J. et al.: *Applied Composite Materials* **2020**, 27, 533.
<https://doi.org/10.1007/s10443-020-09812-8>
- [7] Huszák C., Schramkó M., Kovács T.A.: *Műszaki Tudományos Közlemények* **2023**, 18, 45.
<https://doi.org/10.33894/mtk-2023.18.08>
- [8] Cherolis N.E., Benac D.J., Shaffer D.M. et al.: *Journal of Failure Analysis and Prevention* **2018**, 18(5), 1143.
<https://doi.org/10.1007/s11668-018-0504-7>
- [9] Fedulov B.N., Fedorenko A.N., Lomakin E.V.: *IOP Conference Series: Materials Science and Engineering* **2019**, 581(1), 12023.
<https://doi.org/10.1088/1757-899X/581/1/012023>
- [10] Pandian A., Hameed Sultan M. T., Marimuthu U. et al.: "Low Velocity Impact Studies on Fibre-Reinforced Polymer Composites and Their Hybrids – Review," in "Encyclopedia of Renewable and Sustainable Material, vol. 5" (editors Hashmi S., Choudhury I.A.), Elsevier, Amsterdam 2019, p. 119.
<https://doi.org/10.1016/B978-0-12-803581-8.11289-5>
- [11] Soykök İ.F.: *Academic Platform – Journal of Engineering and Science* **2018**, 6(2), 45.
<https://doi.org/10.21541/apjes.388080>
- [12] Chang Y., Wen W., Xu Y. et al.: *Thin-Walled Structures* **2022**, 177, 109361.
<https://doi.org/10.1016/j.tws.2022.109361>
- [13] Mansour G., Tzikas K., Tzetzis D. et al.: *Applied Mechanics and Materials* **2016**, 834, 173.

- <https://doi.org/10.4028/www.scientific.net/AMM.834.173>
- [14] Soykök İ.F., Ozcan A.R., Tas H.: *Materials Research Express* **2019**, 6(5), 55307.
<https://doi.org/10.1088/2053-1591/ab0151>
- [15] Minak G., Abrate S., Ghelli D. et al.: *Composites Part B: Engineering* **2010**, 41(8), 637.
<https://doi.org/10.1016/j.compositesb.2010.09.021>
- [16] Soykök İ.F., Tas H., Ozdemir O. et al.: *Polymers and Polymer Composites* **2021**, 29(6), 617,
<https://doi.org/10.1177/0967391120930107>
- [17] da Silva J.E.L., Paciornik S., d'Almeida J.R.M.: *Polymer Testing* **2004**, 23(5), 599.
<https://doi.org/10.1016/j.polymertesting.2003.10.008>
- [18] Santulli C.: *NDT and E International* **2001**, 34(8), 531.
[https://doi.org/10.1016/S0963-8695\(01\)00013-5](https://doi.org/10.1016/S0963-8695(01)00013-5)
- [19] Wang S.-X., Wu L., Ma L.: *Materials and Design* **2010**, 31(1), 118.
<https://doi.org/10.1016/j.matdes.2009.07.003>
- [20] Prichard J.C., Hogg P.J.: *Composites* **1990**, 21(6), 503.
[https://doi.org/10.1016/0010-4361\(90\)90423-T](https://doi.org/10.1016/0010-4361(90)90423-T)
- [21] Kinsey A., Saunders D.E.J., Soutis C.: *Composites* **1995**, 26(9), 661.
[https://doi.org/10.1016/0010-4361\(95\)98915-8](https://doi.org/10.1016/0010-4361(95)98915-8)
- [22] de Freitas M., Reis L.: *Composite Structures* **1998**, 42(4), 365.
[https://doi.org/10.1016/S0263-8223\(98\)00081-6](https://doi.org/10.1016/S0263-8223(98)00081-6)
- [23] Mouritz A.P., Gallagher J., Goodwin A.A.: *Composites Science and Technology* **1997**, 57(5), 509.
[https://doi.org/10.1016/S0266-3538\(96\)00164-9](https://doi.org/10.1016/S0266-3538(96)00164-9)
- [24] Zhang Z.Y., Richardson M.O.W.: *Composite Structures* **2007**, 81(2), 195.
<https://doi.org/10.1016/j.compstruct.2006.08.019>
- [25] Shim V.P.W., Yang L.M.: *International Journal of Mechanical Sciences* **2005**, 47(4-5), 647.
<https://doi.org/10.1016/j.ijmecsci.2005.01.014>
- [26] Piggott M.R.: "Load Bearings Fibre Composites, 2nd edition", Kluwer Academic Publishers, Dordrecht 2002. p. 259.
- [27] Günöz A., Kur M., Kara M.: *Polymer Composites* **2024**, 45(13), 12481.
<https://doi.org/10.1002/pc.28650>
- [28] Targino T., Cunha R., Freire Júnior R. et al.: *Journal of Composite Materials* **2024**, 58(23), 2555.
<https://doi.org/10.1177/00219983241274617>
- [29] Barcikowski M., Królikowski W., Lenart S.: *Polimery* **2021**, 62(9), 650.
<https://doi.org/10.14314/polimery.2017.650>
- [30] Zhao S., Gao X., Lou J. et al.: *e-Polymers* **2024**, 24(1), 20240044.
<https://doi.org/10.1515/epoly-2024-0044>
- [31] Dahmene F., Yaacoubi S., Mountassir M.E.L.: *Physics Procedia* **2015**, 70, 599.
<https://doi.org/10.1016/j.phpro.2015.08.031>
- [32] de Groot P.J., Wijnen P., Janssen R.: *Composites Science and Technology* **1995**, 55(4), 405.
[https://doi.org/10.1016/0266-3538\(95\)00121-2](https://doi.org/10.1016/0266-3538(95)00121-2)
- [33] Sayar H., Azadi M., Ghasemi-Ghalebahman A. et al.: *Composite Structures* **2018**, 204, 1.
<https://doi.org/10.1016/j.compstruct.2018.07.047>
- [34] Kumar A.L., Prakash M.: *Iranian Polymer Journal* **2023**, 32(7), 887.
<https://doi.org/10.1007/s13726-023-01171-y>
- [35] Hemanth Raj G., Prakash M., Kumar A.L.: *IOP Conference Series: Materials Science and Engineering* **2020**, 912(3), 032050.
<https://doi.org/10.1088/1757-899X/912/3/032050>
- [36] Vasiliev V.V., Morozov E.: "Advanced Mechanics of Composite Materials. Second edition", Elsevier, Amsterdam 2007.
<https://doi.org/10.1016/B978-0-08-045372-9.X5000-3>
- [37] Duda S., Smolnicki M., Stabla P. et al.: *Thin-Walled Structures* **2024**, 195, 111364.
<https://doi.org/10.1016/j.tws.2023.111364>
- [38] Fang P., Xu Y., Yuan S. et al.: "Investigation on Mechanical Properties of Fiberglass Reinforced Flexible Pipes Under Torsion.", Materials from the ASME 2018 37th International Conference on Ocean, Spain, Madrid, June 17–22 2018.
<https://doi.org/10.1115/OMAE2018-77354>
- [39] Wilhelmsson D., Mikkelsen L.P., Fæster S. et al.: *Composites Part A: Applied Science and Manufacturing* **2019**, 119, 283.
<https://doi.org/10.1016/j.compositesa.2019.01.018>
- [40] He R., Cheng L., Gao Y. et al.: *Composites Science and Technology* **2023**, 244, 110307.
<https://doi.org/10.1016/j.compscitech.2023.110307>
- [41] Davidson P., Waas A.M.: *Mathematics and Mechanics of Solids* **2016**, 21(6), 667.
<https://doi.org/10.1177/1081286514535422>
- [42] Xun L., Mosleh Y., Sun B. et al.: *Composites Science and Technology* **2024**, 252, 110615.
<https://doi.org/10.1016/j.compscitech.2024.110615>
- [43] Wang D., Liao B., Hao C. et al.: *International Journal of Hydrogen Energy* **2021**, 46(23), 12605.
<https://doi.org/10.1016/j.ijhydene.2020.12.177>

Received 20 XI 2024.

Accepted 7 XII 2024.